DOI: 10.15480/882.9356

Eighth International Symposium on Marine Propulsors
smp'24, Berlin, Germany, March 2024

Performance Analysis of Propellers: Improved Coupling of BEM with X-foil

Thomas S. Wu[1], **Spyros A. Kinnas**[1]

[1]Ocean Engineering Group, Department of Civil, Architecture and Environmental Engineering, University of Texas at Austin, Texas, USA

ABSTRACT

The Boundary element method (BEM) is commonly utilized in the hydrodynamic calculation for propellers due to its relatively lower computational demand while simultaneously offering high fidelity. However, the BEM is based on the inviscid potential theory, and typically, the effect of viscosity is considered by either applying a constant empirical friction coefficient or adopting the local friction coefficient calculated by the ITTC-1957 formulation over the blade. Although both methods enhance the correlation of predicted open water characteristics, neither of them takes into account the development of the boundary layer. This study presents a 3D potential-based BEM coupling with a primarily 2D boundary layer solver, X-foil, known as the viscous/inviscid interactive (VII) method. This approach is intended to more accurately evaluate the effects of viscosity on the blade and predict open water characteristics. When applying the VII method to propellers, the boundary layer equations are solved on individual sections of the blade in an iterative manner. The model assumes that boundary layer growth mainly occurs in the streamwise direction within a constant radius but with considering the interaction effects from other sections and blades. Specifically, the original 2D influence coefficients in X-foil have been replaced by the 3D influence coefficients corresponding to the effects of boundary layer sources from panels at each strip and blade. Moreover, the model includes the effects of potentials due to other strips arising from the 3D formulations. The pressure distributions, skin friction coefficients on each blade section, and the open water characteristics of the propeller are compared either with full-blown Reynolds Averaged Navier-Stokes (RANS) simulations or experimental measurements. The results show that the predicted viscous pressure distributions at both the leading and trailing edges are markedly improved by accounting for the effects of potentials from other strips. This model demonstrates robustness and efficiency in predicting viscous effects and requires significantly less computational effort than the intensive 3D meshwork by RANS calculations.

Keywords

Boundary element method, Viscous/inviscid interactive method, Pressure distribution, Friction coefficient.

1 INTRODUCTION

The prediction of propeller performance is a crucial challenge in the marine propeller industry. With the rising demand for larger and more specialized vessels, the installation of more sophisticated propulsion systems that provide high efficiency has become a priority. The boundary element method (BEM) has been extensively used for solving flow around propellers due to its low computational demands and satisfactory accuracy (Moulijn 2015). The primary limitation of the BEM arises from its derivation from inviscid potential flow theory, which leads to neglect of viscous effects. However, accounting for viscosity is critical in accurately predicting the thrust and torque coefficients, efficiency, and in determining the pressure distributions on the propeller blade. The effect of viscosity can be considered by applying an empirical drag-to-lift ratio with a correction to the blade's pitch angle (Kerwin and Lee 1978; Kerwin et al. 1987), or by utilizing the ITTC-1957 formulation at each radial strip on the blade to obtain the friction coefficient. While these methods may provide reasonable results for simple blade geometries, they may not be accurate for those with complicated geometries where the flow around the body becomes more complex. Although RANS simulations calculate most fluid physics, their practical application is constrained by computational costs. Therefore, it is highly desirable to have a rational approach to account for the effect of viscosity by considering boundary layer development while still maintaining low computational demands.

Drela (1989) introduced a vorticity streamfunction panel method coupled with a two-dimensional (2D) viscous/inviscid interaction (VII) solver, X-foil, to account for the effects of viscosity. Nishida and Drela (1995), Milewski (1997), and Mughal (1998) developed numerical schemes that coupled potential flow methods with three-dimensional (3D) boundary layer solvers. However, it is worth noting that applying these schemes to complex propulsor devices is a challenging task due to their demanding computational requirements. In the 3D propeller case, Jessup (1989) conducted experiments on Propeller DTMB 4119 and observed that the development of the boundary layer in the streamwise direction is much more signifi-

cant than in the spanwise direction. Based on the observation from Jessup, Hufford et al. (1994) proposed a coupled scheme for 3D propellers. This scheme coupled a 3D potential-based panel method with a 2D boundary layer solver, X-foil. Notably, this scheme replaced the 2D source influence coefficient with a 3D source in the 2D boundary layer formulations and was applied to each strip along the constant radius of the blade.

Sun and Kinnas (2008) coupled a low-order, potential-based panel method, PROPCAV, with X-foil, following Hufford's method. However, this coupled scheme was limited to considering 2D sources at each strip. Yu (2012), Kinnas et al. (2012), Kinnas et al. (2013), and Purohit (2013) further improved PROPCAV/X-foil by using 3D influence coefficients instead of 2D in the boundary layer equations and considered the effect of the boundary layer from other strips. Kim et al. (2018), Du and Kinnas (2019), and Wu et al. (2023) applied PROPCAV/X-foil to wings, open propellers, and ducted propellers. The results indicated that the coupled method significantly improved the prediction of pressure distribution, especially in the region close to the trailing edge. However, it is important to note that the results only considered the 3D source effect, neglecting the 3D dipole effect from other strips.

Therefore, the objective of this study is to improve the coupled scheme by incorporating the 3D dipole term into the coding and applying it to the DTMB 4381 propeller. The results will be compared with those obtained from Reynolds-averaged Navier Stokes (RANS) simulations and the experimental data.

2 METHODOLOGY

The viscous/inviscid interactive (VII) method is developed by coupling a 3D inviscid solver, PROPCAV, and a 2D boundary layer solver, Xfoil. This section provides a summary of the method.

2.1 PROPCAV

PROPCAV is a 3D low-order Boundary Element Method (BEM). It assumes an inviscid and irrotational flow around the propeller. Thus, the total velocity $\vec{q}$ can be expressed as:

$$\vec{q}(x,y,z,t) = \vec{q}_{\text{in}}(x,y,z,t) + \nabla\phi(x,y,z,t) \tag{1}$$

Where $\vec{q}_{\text{in}}$ represents the incoming flow, and $\nabla\phi$ is the perturbation velocity. This perturbation velocity can be treated as the potential flow governed by Laplace's equation:

$$\nabla^2\phi = 0 \tag{2}$$

with ϕ representing the perturbation potential. The inviscid solution for the discretized propeller geometry can be carried out by expressing the potential ϕ_p at an arbitrary point p using Green's third identity:

$$2\pi\phi_p = \iint_{S_p}\left[\phi_{p'}\frac{\partial G(p,p')}{\partial n_{p'}} - G(p,p')\frac{\partial \phi_{p'}}{\partial n_{p'}}\right]ds + \iint_{S_w}\Delta\phi_w\frac{\partial G(p,p')}{\partial n_{p'}}ds \tag{3}$$

Where S_p refers to the propeller's surface, S_w the trailing wake's surface, G is Green's function, defined as $1/R(p,p')$ in 3D and $2lnR(p,p')$ in 2D, and R is the distance between the field point p and the variable point p'. $\Delta\phi_w$ is the wake strength due to the potential jump at the trailing edge of the blade. In order to obtain an unique solution of Equation (3), the boundary conditions are applied:

1. Since there cannot be any flow through the blade surface, the kinematic boundary condition states:

$$\frac{\partial\phi}{\partial n} = \vec{n}\cdot\nabla\phi = -\vec{q_{in}}\cdot\vec{n} \tag{4}$$

   Where $\vec{n}$ is the normal vector on the blade surface pointing into the flow field.

2. At the trailing edge of the blade, the Kutta condition requires the velocity to be finite.

$$|\nabla\phi| < \infty \text{ at the trailing edge} \tag{5}$$

3. The perturbation velocity far away from the blade should vanish.

$$\nabla\phi \to 0 \tag{6}$$

2.2 Wall Transpiration Model

To simulate viscous effects, the extra boundary layer sources with the unknown strength σ are added onto both the blade and wake surfaces, known as the wall transpiration model. In 2D flows, the modified discretized form of Equation (3) can be expressed as follows:

$$\sum_{j=1}^{N} A_{ij}\phi_j = \sum_{j=1}^{N} S_{ij}\left(\frac{\partial\phi}{\partial n}\right)_j + \sum_{j=1}^{N+N_w} B_{ij}\sigma_j \tag{7}$$

The source strength can be shown to be related to the boundary layer variables, the edge velocity and the displacement thickness in Hufford (1994).

$$\sigma = \frac{\partial m}{\partial s} = \frac{\partial(U_{vis}\delta^*)}{\partial s} \tag{8}$$

The potentials obtained from Equation (7) are viscous potentials. In viscous cases, the total potential should be the sum of the viscous potential and the inflow potential. When differentiated along the streamwise direction, it yields the viscous velocity or the edge velocity, which can be substituted into the boundary layer equations.

$$U_i^{vis} = U_i^{inv} + \sum_{j=1}^{N+N_w} C_{ij}\sigma_j \tag{9}$$

Where U_i^{vis} is the edge velocity on the i panel, N and NW are the number of elements on the body surface S_p, and the wake surface S_w, C_{ij} is the 2D source influence coefficient matrix, and σ_j is the boundary layer source strength on the j panel.

In terms of propeller cases, assuming boundary layer growth in the chordwise direction, the 3D body can be divided into K strips in the spanwise direction. By replacing

the 2D influence coefficient with the 3D influence coefficient, the boundary layer effect can be taken into account from other strips. Since it contains more unknowns in the expression of 3D edge velocity, this 3D model is solved iteratively for the extra unknowns. A detailed derivation of the 3D formulations can be found in Du (2019). The viscous velocity on the K-th strip is given by:

$$U_K^{vis} = U_K^{inv} + D_K A_{KK}^{-1} B_{KK} \sigma_K + \sum_{j=1, j\neq K}^{M} D_K A_{KK}^{-1} B_{Kj} \sigma_j + \sum_{j=1, j\neq K}^{M} D_K A_{KK}^{-1} A_{Kj} [\phi_J^{inv} - \phi_J^{vis}] \quad (10)$$

Where M indicates the strip number along the spanwise direction, D_K refers to the differentiation matrix for the arclength on the K-th strip, A represents the matrix of the dipole influence coefficients, and B represents the matrix of the blowing source influence coefficients. The first line of Equation (10) accounts for the edge velocity along with the influence of the boundary layer sources from the K-th strip, which closely resembles the 2D form in Equation (9). The second line in Equation (10) represents the effect of the boundary layer sources of other strips, and the final line considers the dipoles from other strips, which was omitted in the presentation of results of Wu et al. (2023).

2.3 Viscous/inviscid interactive method

In order to determine the sources of the boundary layer, a boundary layer solver, X-foil, has been employed to provide a viscous/inviscid coupling. The viscous equations, as described in Drela (1989), will be briefly summarized here. When applying the viscous/inviscid interactive (VII) method to a propeller, it is assumed that the dominating viscous effect on the propeller blade is in the chordwise direction, the boundary layer equations employ the 2D integral momentum and kinetic energy equations:

$$\frac{d\theta}{ds} + \left(2 + H - M_e^2\right) \frac{\theta}{U_e} \frac{dU_e}{ds} = \frac{C_f}{2} \quad (11)$$

$$\theta \frac{dH^*}{ds} + H^* \left(1 - H\right) \frac{\theta}{U_e} \frac{dU_e}{ds} = 2C_D - H^* \frac{C_f}{2} \quad (12)$$

Where Mach number $M_e = 0$ for the incompressible flow, U_e the edge velocity, θ the momentum displacement of the boundary layer, H the shape parameter, H^* the kinetic energy shape parameter, and C_f defined as the skin friction coefficient:

$$C_f = \frac{\tau_w}{\frac{1}{2}\rho U_e^2} \quad (13)$$

The boundary layer parameters can be determined iteratively by coupling Equations (11) and (12) with a third closure equation, depending on the laminar or turbulent flow.

Closure for laminar flows

$$\frac{d\tilde{n}}{ds} = \frac{d\tilde{n}}{dR_{e\theta}}(H_K) \frac{dR_{e\theta}}{ds}(H_k, \theta) \quad (14)$$

Closure for turbulent flows

$$\frac{\delta}{C_\tau} \frac{dC_\tau}{ds} = 5.6[C_{\tau EQ}^{1/2} - C_\tau^{1/2}] + 2\delta \left\{ \frac{4}{3\delta^*} \left[\frac{C_f}{2} - \left(\frac{H_k - 1}{6.7 H_k} \right)^2 \right] - \frac{1}{U_e} \frac{dU_e}{ds} \right\} \quad (15)$$

Where δ represents the boundary layer thickness, δ^* the displacement thickness, H_K the kinematic shape function, and $\tilde{n}$ is the most-amplified of the Tollmien-Schlichting wave.

3 RESULTS

The present coupled scheme, PROPCAV/X-foil, is applied to a five-blade propeller, the DTMB 4381 propeller, as shown in Figure 1. The design advance ratio $J_s = V_s/nD$ of the propeller is 0.889. The results are compared with experiment values from Boswell (1971) and RANS simulations from $ANSYS/Fluent$.

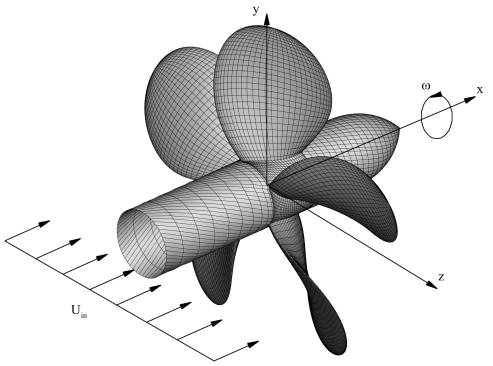

Figure 1: Propeller geometry under uniform inflow U_{in}, modeled by PROPCAV/X-foil; the x, y, and z axes represent the propeller fixed coordinate system.

Before any further analysis, a grid convergence study is carried out to validate the present model. The number of panels in the chordwise and spanwise directions, varying from 50 to 70 and 20 to 40, is examined. Table 1 presents a comparison of thrust and torque coefficients. The thrust and torque coefficients are defined as follows:

$$K_t = \frac{T}{\rho n^2 D^4} \quad (16)$$

$$K_q = \frac{Q}{\rho n^2 D^5} \quad (17)$$

The results indicate that increasing the number of chordwise and spanwise panels leads to reduced discrepancies between the present model and the experiment. The torque values for the 60x30 and 60x40 configurations are nearly identical, although there is a slight increase in error compared to the experimental data for the 60x40 case. While all cases exhibit a slight overprediction in thrust and torque coefficients, it is important to note that the errors for all cases remain below 5%, which ensures the accuracy of the results. The 60x30 panel configuration has been selected for subsequent analysis with RANS simulations and experiment comparisons.

Case	Kt	Error (%)	$10Kq$	Error (%)
50x20	0.2150	3.38	0.4660	4.71
60x20	0.2147	3.22	0.4631	4.07
70x20	0.2142	3.01	0.4630	4.06
60x30	0.2117	1.81	0.4594	3.24
60x40	0.2109	1.42	0.4601	3.41
Exp.	0.208	-	0.445	-

Table 1: Comparison of thrust and torque coefficients of Propeller 4381 at $J_s = 0.889$

Figure 2 shows the domain and boundary conditions for RANS simulations. To increase computational efficiency, a periodic boundary condition is applied, reducing the needed domain size to one-fifth of the original and resulting in a total number of 5.37 million hexahedral cells. The $k-\omega$ SST turbulent model is employed to predict near-wall flows with a Reynolds number of $6.22e5$. The Reynolds number is based on the propeller diameter, $R_{eD} = V_s D/\nu$, where ν represents the kinematic viscosity of the fluid. The spatial discretization applies the QUICK scheme, and the pressure correction is implemented using the SIMPLEC method.

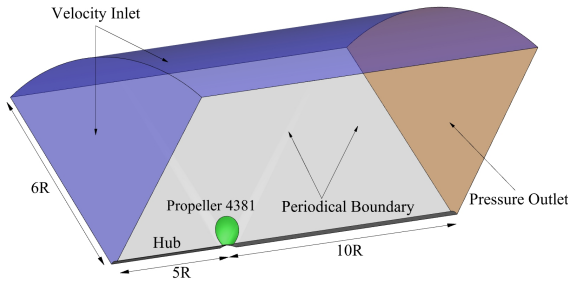

Figure 2: The RANS domain and the boundary conditions used in the simulation

Figure 3 presents detailed pressure comparisons for different strips at $r/R = 0.5$, $r/R = 0.7$, and $r/R = 0.9$ of propeller 4381 at $J_s = 0.889$. In propeller case, the pressure coefficient C_p is defined as

$$-C_p = \frac{p_\infty - p}{\frac{\rho}{2} n^2 D^2} \tag{18}$$

The pressures predicted by the current model exhibit a stronger correlation with the RANS results compared to those predicted by the PROPCAV (Inviscid) and PROPCAV (ITTC-1957), particularly near the trailing edge region of the blade. Approaching the trailing edge, the impact of fluid viscosity becomes more pronounced, resulting in a thicker boundary layer. Consequently, more improvements are observed in this region because of the boundary layer correction. It is important to note that the pressure distribution deviated in the leading-edge region in Wu et al. (2023). This underestimation of the pressure was attributed to the omission of the dipole effect. However, by incorporating the dipole term into the model, the pressure exhibited a good correlation with RANS simulations.

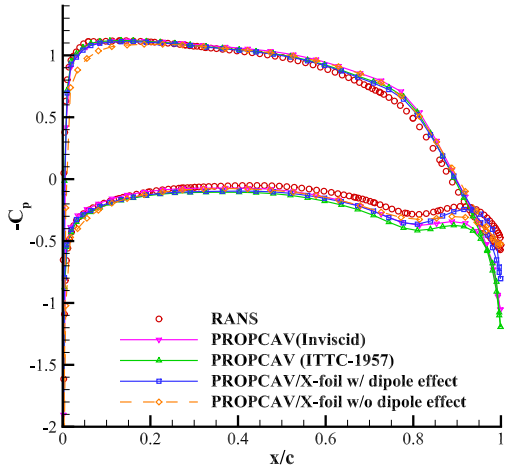

(a) r/R = 0.5

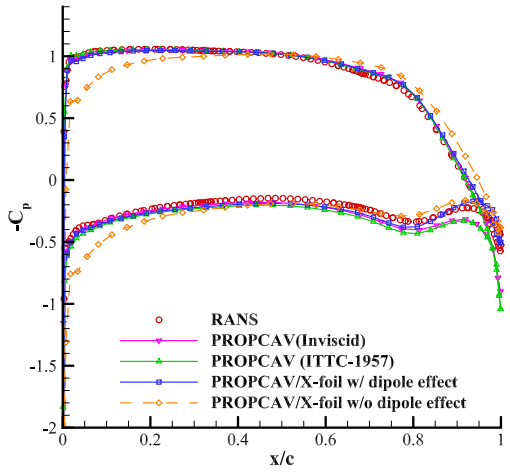

(b) r/R = 0.7

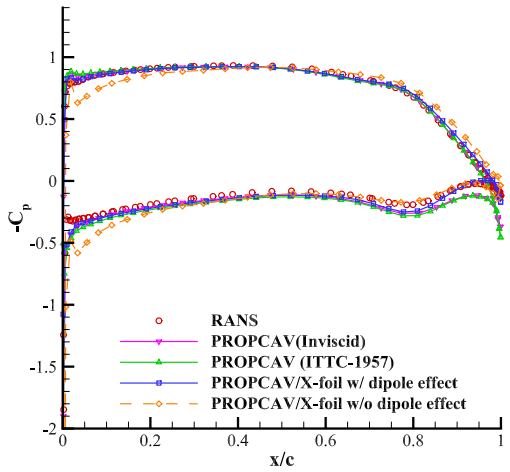

(c) r/R = 0.9

Figure 3: Comparison of pressure coefficients on different strips of Propeller 4381, predicted by RANS, PROPCAV (Inviscid), PROPCAV (ITTC-1957), and PROPCAV/X-foil

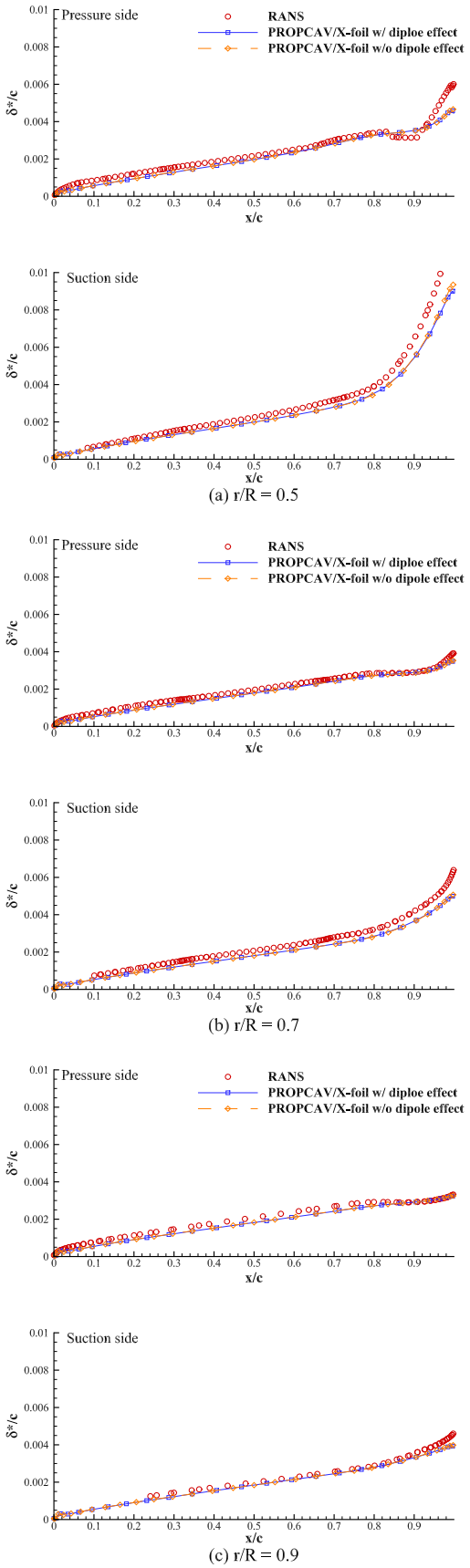

Figure 4: Comparison of displacement thickness on different strips of Propeller 4381, predicted by RANS and PROPCAV/X-foil

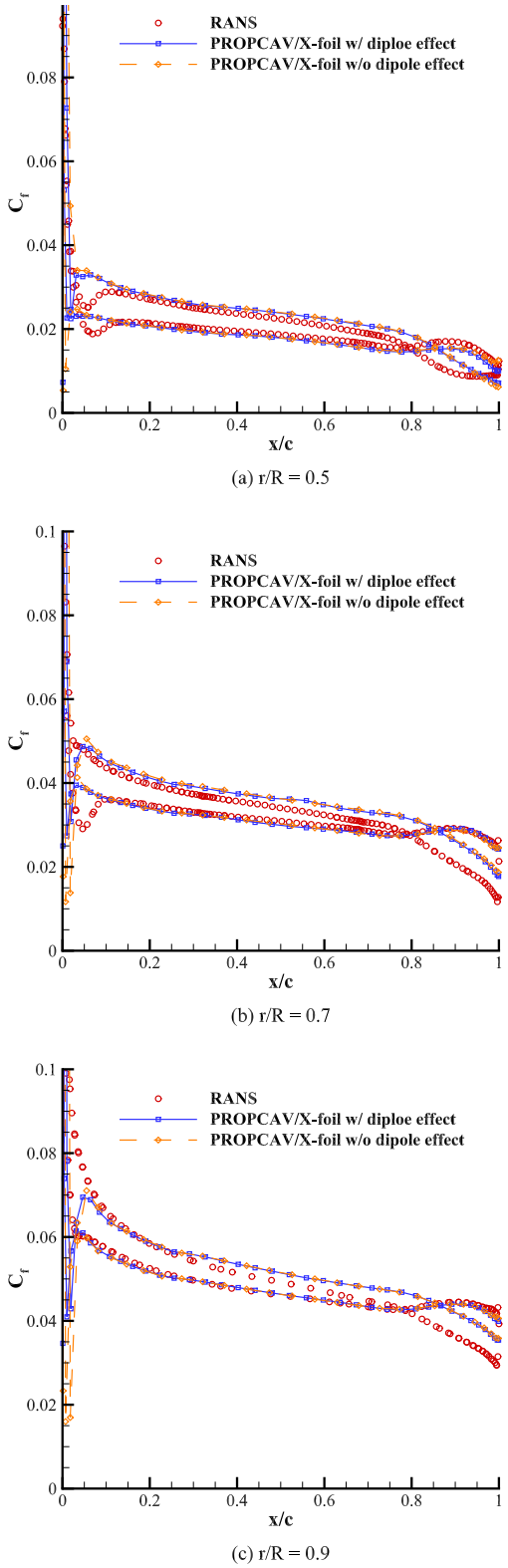

Figure 5: Comparison of skin friction coefficients on different strips of Propeller 4381, predicted by RANS and PROPCAV/X-foil

Figure 4 presents a comparison of the displacement thickness along the strips at $r/R = 0.5$, $r/R = 0.7$, and $r/R = 0.9$ of propeller 4381 at $J_s = 0.889$ predicted by the present model with RANS simulations. The laminar-to-turbulent flow transition points on both the pressure and

suction side of the blade are forced close to the leading edge at $x/c = 0.01$ in PROPCAV/X-foil, while in RANS simulations, the flow field is assumed to be fully turbulent. The comparisons suggest good agreement between PROPCAV/X-foil and RANS simulation on both the pressure and suction sides. It is observed that the integration of the dipole term into the model has a minimal impact on the prediction accuracy.

In propeller cases, predicting the thrust and torque is of importance. These quantities, attributed to fluid viscosity, are calculated by integrating the shear stress τ on the blade surfaces. Figure 5 illustrates the comparison of skin friction at different radial positions, $r/R = 0.5$, $r/R = 0.7$, and $r/R = 0.9$, for propeller 4381 at $J_s = 0.889$ predicted by the present VII method and RANS simulations. Notably, results near the leading edge on both the suction and pressure sides exhibit regional discrepancies between PROPCAV/X-foil and RANS. It is possibly because the VII method requires a smooth transition from laminar to turbulent flow. Therefore, regardless of forcing the transition point at $x/c = 0.01$, more distance is required to develop the boundary layer. As the flow becomes fully developed, the results display an acceptable agreement compared to RANS simulations, and suggest a more reasonable C_f than using an empirical constant to correct the viscous effect in PROPCAV (Inviscid), or the local friction coefficient based radial positions calculated using the ITTC-1957 formulation.

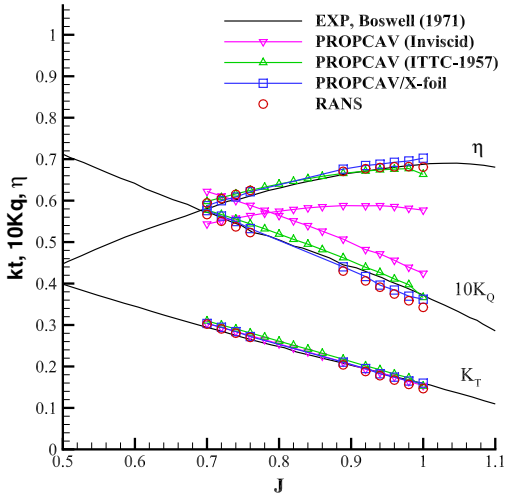

Figure 6: Comparison of thrust, torque, and efficiency at different advance ratios of Propeller 4381, predicted by experiments, RANS, PROPCAV, and PROPCAV/X-foil

The comparison of predicted viscous thrust and torque coefficients, as well as efficiency, is carried out over a range of advance ratios from $J_s = 0.7$ to 1.0, as shown in Figure 6. The VII method significantly enhances the correlation between the predicted torque and the experimental data in contrast to the pure BEM without boundary layer corrections, leads to a more accurate prediction of efficiency. The absence of data points between $J_s = 0.76$ and 0.88 is attributed to convergence issues with the VII method. This could be due to either the convergence criteria not being met or computational instability causing the calculations to fail.

Table 2 shows the comparison of the computational time between PROPCAV/X-foil and RANS simulations at $J_s = 0.889$. All calculations were carried out on FRONTERA cluster at Texas Advanced Computing Center, using *Intel Xeon Platinum 8280 @ 2.7Ghz* processors. It is worth noting that the coupling model, PROPCAV/X-foil, exhibits high computational efficiency, completing the calculation in 2.3 minutes, compared to PROPCAV (Inviscid), which takes 1.7 minutes. Moreover, the present model's computational speed is approximately 80 times faster than RANS, not to mention the additional time required for preprocessing and post-processing in RANS simulations.

Case	**# of CPUs**	**Time (min)**
PROPCAV (Inviscid)	56	1.7
PROPCAV/X-foil	56	2.3
RANS	280	35.01

Table 2: Comparison of the computational time between PROPCAV, PROPCAV/X-foil, and RANS simulation

4 CONCLUSIONS

This study introduces an improved coupled scheme by adding the 3D dipole term to the coding to predict boundary layer variables for Propeller propeller 4381. Full-blown RANS simulations are conducted to compare boundary layer variables, pressure distribution, and propeller performance.

The results for both skin friction coefficient and displacement thickness demonstrate a strong correlation with the RANS results. Furthermore, the 3D VII method significantly increased the accuracy of pressure distribution prediction near the trailing edge. By accounting for the dipole effect from other strips, the pressure prediction in the region near the leading edge has also been improved compared to the previous work by Wu et al. (2023).

Finally, the presented coupling method has improved torque prediction that aligns well with experimental data, leading to a more accurate prediction of propeller efficiency.

5 FUTURE WORK

The potential of the 3D VII method has been demonstrated in the paper. The ongoing effort will focus on improving the stability of the boundary layer solver to make it more versatile for propeller performance analysis. Additionally, the study will extend the application of the 3D VII method to encompass ducted turbines and propellers.

ACKNOWLEDGMENTS

Support for this research was provided by the U.S. Office of Naval Research (Grant Number N00014-21-1-2488; Dr. Yin Lu Young) and by Phases IX of the "Consortium on Cavitation Performance of High-Speed Propulsors."

REFERENCES

Boswell, R.J. (1971). 'Design, Cavitation Performance, and Open-Water Performance of a Series of Research Skewed Propellers', Technical Report 3339, Department of the Navy, Naval Ship Research and Development Center.

Drela, M. (1989). 'XFOIL: An analysis and design system for low Reynolds number airfoils', Low Reynolds Number Aerodynamics: Proceedings of the Conference Notre Dame, Indiana, USA, Springer, pp. 1–12.

Du, W. (2019). 'Application of the three-dimensional viscous/inviscid interaction method on predicting the performance of propulsors with blunt trailing edges', Ph.D. Thesis, The University of Texas at Austin.

Du, W., Kinnas, S.A. (2019). 'Applying 3D Viscous/Inviscid Interaction Method to Predict Flows Around Wings and Propellers'. SNAME 24th Offshore Symposium, SNAME.

Hufford, G.S., Drela, M., Kerwin, J.E. (1994). 'Viscous Flow Around Marine Propellers Using Boundary-Layer Strip Theory', Journal of Ship Research **38**(01), pp.52-62 .

Jessup, S.D. (1989). 'An experimental investigation of viscous aspects of propeller blade flow', Ph.D. Thesis, The Catholic University of America.

Kerwin, J.E., Lee, C.S. (1978). 'Prediction of steady and unsteady marine propeller performance by numerical lifting-surface theory', vol. 86. Transactions of Society of Naval Architects and Marine Engineers.

Kerwin J.E., Kinnas S.A., Lee J.T., Shih W.Z. (1987). 'A surface panel method for the hydrodynamic analysis of ducted propellers', SNAME transaction **95**: 93-122.

Kim, S., Kinnas, S.A., Du, W. (2018). 'Panel Method for Ducted Propellers with Sharp Trailing Edge Duct with Fully Aligned Wake on Blade and Duct', Journal of Marine Science and Engineering, **6**(3), p.89.

Kinnas, S.A., Jeon, C.H., Purohit, J., Tian, Y. (2013). 'Prediction of the unsteady cavitating performance of ducted propellers subject to an inclined inflow', International symposium on marine propulsors SMP, Vol.13.

Kinnas, S.A., Yu, X. Tian, Y.(2012). 'Prediction of propeller performance under high loading conditions with viscous/inviscid interaction and a new wake alignment model', Proceedings of the 29th Symposium on Naval Hydrodynamics, Gothenburg, Sweden, pp. 26-31.

Milewski, W.M. (1997). 'Three-dimensional viscous flow computations using the integral boundary layer equations simultaneously coupled with a low order panel method', Doctoral dissertation, Massachusetts Institute of Technology.

Moulijn, J. (2015). 'Application of various computational methods to predict the performance and cavitation of ducted propellers', Fourth International Symposium on Marine Propulsors smp, Vol.15.

Mughal, B.H. (1998). 'Integral methods for three-dimensional boundary layers', Doctoral dissertation, Massachusetts Institute of Technology.

Nishida, B., Drela, M. (1995). 'Fully simultaneous coupling for three-dimensional viscous/inviscid flows', 13th Applied Aerodynamics Conference, p.1806 .

Purohit, J.B. (2013). 'An improved viscous-inviscid interactive method and its application to ducted propellers', Doctoral dissertation, The University of Texas at Austin.

Sun, H., Kinnas, S.A. (2008). 'Performance Prediction of Cavitating Water-Jet Propulsors Using a Viscous/Inviscid Interactive Method', NAME Maritime Convention, SNAME.

Wu, T.S., Kim, S., Kinnas, S.A. (2023). 'Numerical Prediction of Skin Friction Coefficient by Coupling a Bem with X-Foil: Effect on the Hydrofoil and Propeller Performance', SNAME 28th Offshore Symposium, SNAME.

Yu, X. (2012). 'Three dimensional viscous/inviscid interactive method and its application to propeller blades', Doctoral dissertation, The University of Texas at Austin.